Probe for the measurement of cell surface pH in vivo and ex vivo

Michael Anderson[a], Anna Moshnikova[a], Donald M. Engelman[b,1], Yana K. Reshetnyak[a], and Oleg A. Andreev[a,1]

[a]Physics Department, University of Rhode Island, Kingston, RI 02881; and [b]Department of Molecular Biophysics and Biochemistry, Yale University, New Haven, CT 06511

Contributed by Donald M. Engelman, May 27, 2016 (sent for review December 8, 2015; reviewed by Constantinos Koumenis and Peter J. J. Parker)

We have developed a way to measure cell surface pH by positioning a pH-sensitive fluorescent dye, seminaphtharhodafluor (SNARF), conjugated to the pH low insertion peptide (pHLIP). It has been observed that many diseased tissues are acidic and that tumors are especially so. A combination of effects acidifies tumor cell interiors, and cells pump out lactic acid and protons to maintain intracellular pH, acidifying the extracellular space. Overexpression of carbonic anhydrases on cell surfaces further contributes to acidification. Thus, the pH near tumor cell surfaces is expected to be low and to increase with distance from the membrane, so bulk pH measurements will not report surface acidity. Our new surface pH-measurement tool was validated in cancer cells grown in spheroids, in mouse tumor models in vivo, and in excised tumors. We found that the surface pH is sensitive to cell glycolytic activity: the pH decreases in high glucose and increases if glucose is replaced with nonmetabolized deoxyglucose. For highly metastatic cancer cells, the pH measured at the surface was 6.7–6.8, when the surrounding external pH was 7.4. The approach is sensitive enough to detect 0.2–0.3 pH unit changes in vivo in tumors induced by i.p. injection of glucose. The pH at the surfaces of highly metastatic cells within tumors was found to be about 6.1–6.4, whereas in nonmetastatic tumors, it was 6.7–6.9, possibly creating a way to distinguish more aggressive from less aggressive tumors. Other biological roles of surface acidity may be found, now that targeted measurements are possible.

pH low insertion peptide | tumor acidity | fluorescence | SNARF

In this paper, we report a method that allows targeted measurement of cell surface pH in diseased tissues and ex vivo specimens for the first time to our knowledge. Extracellular acidity is associated with the development of various pathological states, such as those in tumors, ischemic stroke, neurotrauma, epileptic seizure, inflammation, infection, wounds, and others (1–3). Insights and therapeutic strategies might be gained by measuring pH with accuracy, precision, and high-spatiotemporal resolution in cell cultures, animal models, and in humans. Extracellular acidosis originates from enhanced glucose uptake and metabolism, known as the Warburg effect. An enhanced use of glycolysis produces cytoplasmic lactic acid and protons, which are intensively pumped out of cells to keep the intracellular pH near neutral (4–6). Carbonic anhydrases on the surfaces of cancer cells further contribute to an acidification of the environment (7, 8). As a consequence, a reversed membrane pH gradient is formed: the extracellular pH surrounding a cancer cell is lower than the intracellular pH, which is opposite to the gradient in normal cells in healthy tissue (9, 10). The average, bulk extracellular pH in tumors is just 0.5–0.8 pH units lower than the extracellular pH in healthy tissue (11); however, the pH is at its lowest at the surfaces of cells (12) and increases with distance from the cellular membrane, becoming normal in the vicinity of blood vessels (13). Thus, the average pH in tissue is less informative regarding cell metabolism than the pH at cell surfaces.

In vivo magnetic resonance spectroscopy (MRS) and MRI have been used to monitor tissue pH changes by using endogenous and exogenous nuclear MR–active compounds (14, 15). Tumor pH has also been measured using hyperpolarized [^{13}C]bicarbonate (16, 17). However, these methods are limited in spatial resolution and cannot measure pH on a cellular level, where optical approaches must be used. Attempts have been made to use fluorescence imaging to study pH near the surface of cultured cancer cells and to monitor behavior of individual fluorescent cancer cells in the heterogeneous microenvironments of tumors (18–22), but in most cases, the pH-sensitive agents were small molecules distributed in an entire organ/tissue and in blood (where the pH is normal) and were washed out from the body very quickly. In other cases, nanocarriers were used (nanoparticles or bacteriophage particles), but cells internalize them readily via endocytotic pathways, so the pH could be reported predominately in endosomes (21). The use of antibody- or receptor-targeting peptides/molecules would also lead to the probes' internalization and removing them from the surface. To measure pH on the surfaces of individual cells, the pH-sensitive probe needs to be located close to the plasma membrane. Lipids or fatty acids conjugated with pH-sensitive probes (19, 23) could be used for pH measurements on a cellular level, but the probes are not selective for cells in a diseased tissue and will incorporate into any cellular membrane. Furthermore, the probes can readily undergo flipping and participate in lipid exchange, thus making the identification of their exact location problematic, especially in experiments in vivo.

We present a novel approach to pH measurements at the surfaces of cells in diseased tissues, based on the use of a pH-sensitive fluorescent dye, seminaphtharhodafluor (SNARF), conjugated to the Lys residues at the N-terminus of a pH low insertion peptide (pHLIP). Peptides of the pHLIP family insert across cell membranes in a pH-dependent manner, with their N-termini exposed to

Significance

In acidic, diseased tissues, such as tumors, cell surfaces are expected to be more acidic than the surroundings, but no means have been available to measure surface acidity specifically in such tissues. We have developed a probe that uses a pH low insertion peptide to locate a pH-sensing dye, seminaphtharhodafluor, at acidic cell surfaces and find that the probe can measure surface pH, which is correlated with tumor aggressiveness. Even an individual cancer cell maintains acidity at its surface and can be detected in a well-perfused area. The new probe can be used in vivo and ex vivo on tissue specimens and opens a path to both medical utility and exploration of other functions of acidity on cell surfaces.

Author contributions: M.A., D.M.E., Y.K.R., and O.A.A. designed research; M.A., A.M., and O.A.A. performed research; M.A., Y.K.R., and O.A.A. analyzed data; and D.M.E., Y.K.R., and O.A.A. wrote the paper.

Reviewers: C.K., University of Pennsylvania; and P.J.J.P., King's College London and Francis Crick Institute.

Conflict of interest statement: O.A.A., D.M.E., and Y.K.R. have financial interests in pHLIP, Inc. O.A.A. and Y.K.R. have disclosed those interests fully to the University of Rhode Island. D.M.E. has disclosed those interests fully to Yale University. O.A.A., D.M.E., and Y.K.R. have in place an approved plan for managing any potential conflicts.

Freely available online through the PNAS open access option.

[1]To whom correspondence may be addressed. Email: andreev@mail.uri.edu or donald.engelman@yale.edu.

the extracellular space and their C-termini in the cytoplasm (24–27). The molecular mechanism of a pHLIP action is based on the protonation of Asp/Glu residues, which enhances peptide hydrophobicity and promotes membrane-associated folding and insertion of a transmembrane helix (28, 29). pHLIPs labeled with optical, PET or single-photon emission computed tomography probes target acidic diseased tissue and are considered to be novel acidity markers (30–37). The tool we present here for measuring the pH at the extracellular surface of a cell might contribute to understanding disease progression and to the development of approaches using pH-based, image-guided interventions.

Results

We have developed a tool for pH measurement at the surfaces of cells and validated it on liposomes in vitro, on tumor spheroids grown from different cancer cell lines, using mouse tumor models in vivo, and on human tumor tissue samples examined ex vivo. As noted above, we are using a pHLIP to target and localize a pH-sensitive dye at the surface of a tumor cell. In addition to the titratable groups in the transmembrane region, the pHLIP has multiple protonatable residues at its membrane-inserting C-terminal end, which are deprotonated in the cytoplasm and serve as additional anchoring points for the peptide in membrane. Thus, once pHLIP is inserted into a plasma membrane, the rate of its exit from membrane is very low even when the extracellular pH is raised, creating an opportunity to treat cells with the pHLIP at low pH and then to raise the extracellular for measurements. The N-terminus of the peptide was acetylated and the adjacent sequence contained a single Lys residue, allowing specific conjugation with a SNARF-1 dye, followed by activation of SNARF-1 at a highly basic pH to obtain SNARF-pHLIP. The product was purified and characterized.

The ratiometric pH indicator SNARF allows pH to be measured independently of the dye's concentration, by comparing the fluorescence peaks at two wavelengths. The dye has been used previously to measure pH in vivo (22). The SNARF-pHLIP was excited by the xenon lamp attached to an inverted epifluorescence microscope in the range of 531 ± 20 nm, as selected by an excitation filter. The fluorescence was selected by an emission cutoff filter for the detection of light at wavelengths longer than 580 nm. By connecting a spectrograph to the microscope, we were able to record the entire fluorescence spectrum of SNARF from 500 to 800 nm simultaneously. The spectra were analyzed to establish the ratio of emission at 595 to that at 645 nm. In contrast to the acquisition of separate images at the two wavelengths via different filters, measurements of continuous spectra allow us to simultaneously visualize changes in the spectral components of protonated and deprotonated forms of the SNARF dye and avoids any potential problems related to photobleaching because both peaks would decrease proportionally and their ratio would not change.

We grew tumor spheroids from the highly metastatic human cervical adenocarcinoma, HeLa, and two human melanoma cell lines, M4A4 and NM2C5, where M4A4 is highly metastatic, whereas NM2C5 is nonmetastatic (38, 39). Fig. 1 *A* and *B* shows representative fluorescence images obtained via two different filter sets of a tumor spheroid stained with the SNARF-pHLIP. Fig. 1*C* shows the same spheroid stained with DAPI to visualize cell nuclei. Because our main goal was to measure pH at the surfaces of cells, we had to prove that SNARF is indeed located in the extracellular space, and not taken up by endocytosis. We imaged cells in HeLa tumor spheroids before (Fig. 1*D*) and immediately after (Fig. 1*E*) treatment with Trypan blue, which is membrane-impermeable and capable of quenching the emission of fluorophores in the range of 500–600 nm (40). The fluorescence of the SNARF-pHLIP in this region was completely quenched, indicating that SNARF is located in the extracellular space. The spectra of the SNARF-pHLIP before and after addition of Trypan blue are shown on Fig. 1*F* (the emission at 680 nm is associated with Trypan blue, and the vast majority of cells were viable).

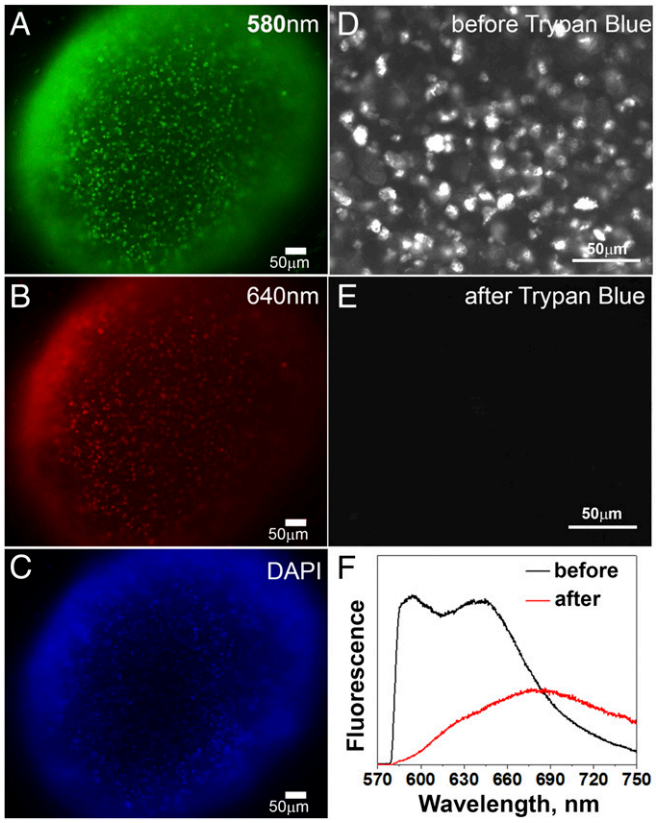

Fig. 1. Images of tumor spheroids and Trypan blue assay. (*A* and *B*) Fluorescence images of HeLa tumor spheroids treated with the SNARF-pHLIP at pH 6.6 were acquired using 580 ± 7 nm (*A*) and 640 ± 7 nm (*B*) emission filters. (*C*) Each spheroid was then treated with DAPI to stain cell nuclei (colors are artificial; 10× objective lens). (*D* and *E*) The SNARF-pHLIP images of HeLa tumor spheroids are shown before (*D*) and immediately after (*E*) the addition of 0.67 M of Trypan blue, acquired via a 580 ± 7 nm emission filter. (*F*) Spectra of SNARF-pHLIP–treated HeLa tumor spheroids before and after treatment with Trypan blue.

It was necessary to create a calibration curve to convert 595/645 nm ratio values into pH values. The ratio of emission at 595 to 645 nm was calculated from the fluorescence spectra of the SNARF-pHLIP bound to 1-palmitoyl-2-oleoyl-*sn*-glycero-3-phosphocholine (POPC) liposomes at various pH values, which were recorded under a microscope (using exactly the same settings as in other experiments) (Fig. 2*A*). The ratios established a calibration curve (Fig. 2*B*). Upon mixing, the pH equilibrates rapidly in the solution, at the surfaces of liposomes, where most of the SNARF-pHLIP is located, and inside the liposomes (29, 41). From the curve, we obtain:

$$\mathrm{pH} = (8.459 \pm 0.031) - (1.223 \pm 0.024) \times \mathrm{ratio}_{595/645}. \qquad (1)$$

To confirm that the calibration curve obtained on liposomes is applicable to cells, tumor spheroids were treated with 50 mM 2-deoxyglucose (2DG), a nonmetabolizable analog of glucose that inhibits fermentative metabolism and hence the proton production and proton flux, as confirmed previously using the Seahorse extracellular flux analyzer (42). As expected, all three cell lines grown in spheroids and treated with 2DG exhibited the same ratio of fluorescence at 595/645 nm, coinciding with the ratios obtained on liposomes (Fig. 2*C*).

The calibrated SNARF-pHLIP was used to measure pH at the surface of metastatic (HeLa and M4A4) and nonmetastatic (NM2C5) cancer cells grown in tumor spheroids in the presence of 50 mM glucose, which enhances and promotes cellular metabolism

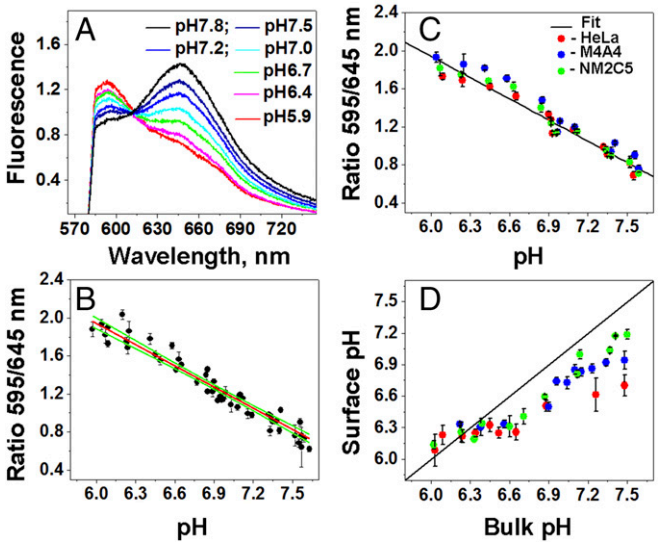

Fig. 2. Calibration curves and pH at the surfaces of cancer cells in tumor spheroids. (*A*) Emission spectra at different pH values of liposomes treated with the SNARF-pHLIP in PBS containing 50 mM 2-DG were recorded using an inverted epifluorescence microscope connected to a spectrograph. (*B*) The calibration curve (red line) and 95% confidence interval (green lines) were obtained by linear fitting of 595/645 fluorescence ratios (black circles) of the SNARF-pHLIP bound to POPC liposomes at various pH values. A separate cell-based calibration curve in 50 mM 2-DG was obtained as a function of pH from HeLa, M4A4, and NM2C5 cell spheroids treated with the SNARF-pHLIP in PBS. (*C*) Shown are the 595/645 nm ratio values and the fit (black line). Cellular surface pH values in glucose for HeLa, M4A4, and NM2C5 cell spheroids were then obtained using the calibration spectra. (*D*) Spheroids were treated with the SNARF-pHLIP in PBS containing 50 mM glucose at different pH values.

(Fig. 2*D*). Note that the pH at the surface of metastatic cancer cells does not increase to more than pH 7.0, even when the pH of the bulk solution is around 7.5. Furthermore, nonmetastatic cancer cells are slightly less acidic than metastatic cells, especially in the range of normal pH values. With a decrease of pH, we observed equilibration of cell surface pH and the bulk external solution at pH $\leq$ 6.4.

The advantage of our approach is its applicability for pH measurements in vivo, because the pHLIP can target acidic diseased tissue and tether imaging agents, including fluorescence markers, to the surfaces of cells (31). To validate this approach in vivo, we grew tumors in mice using the same cell lines studied in the spheroids (above): metastatic HeLa and M4A4 and, less metastatic, NM2C5. When the tumors reached about 5–8 mm in diameter, food was withdrawn for 24 h to reduce the supply of glucose to cancer cells from the blood, thereby increasing tumor pH as much as possible, followed by a single i.v. injection of the SNARF-pHLIP construct. At 4 h postinjection, the mouse was anesthetized and the skin was removed from the tumor site. Fluorescence spectra and images were recorded from the tumor surface. Then, each mouse was given a single i.p. injection of glucose solution. It was shown previously that the average extracellular pH decreases after glucose administration and reaches a minimum level 0.2–0.3 pH units below the initial value (43). We measured spectral changes for more than 40 min after the injection of glucose (Fig. 3*A*). The measurements showed acidification of the tumors, with no further changes after 40 min. Fig. 3*B* shows the mean of the cellular surface pH in live animals before and after glucose injection. HeLa tumors were the most acidic even after the 24 h starvation period. A statistically significant 0.3 pH unit reduction of the surface pH was observed in M4A4 metastatic tumors, whereas no significant changes were monitored for the NM2C5 nonmetastatic tumors after glucose injection. Finally, the animals were euthanized, tumors were excised and cut in half, and fluorescence was recorded from the centers of the tumor. The cellular surface pH values in the centers of HeLa, M4A4, and NM2C5 tumors were found to be 6.5 $\pm$ 0.2, 6.7 $\pm$ 0.5, and 6.9 $\pm$ 0.3, respectively, with some HeLa and M4A4 tumors having regions with surface pH values as low as pH 6.0–6.1.

Finally, we analyzed tumor tissues excised from mice, immediately treated with the SNARF-pHLIP ex vivo for 1 h, extensively washed with pH 7.4 PBS buffer, and observed using SNARF fluorescence spectra and images (Fig. 3*C*). The incubation treatment was performed in the absence and presence of glucose. Glucose in solution promotes cellular metabolism selectively in glycolytic, highly metastatic cancer cells and enhances acidity near cellular surfaces. Thus, pHLIP preferentially inserts into plasma membrane of cells with low pH at the surface, such as cancer cells. At the same time, it is known that glucose does not affect significantly nonglycolytic cells in healthy tissue, which have normal surface pH (44). The mean values of the cellular surface pH in highly metastatic human HeLa and murine 4T1 mammary tumor samples in the absence and presence of glucose are shown in Fig. 3*D*. The measured surface pH was lowered by 0.7 and 0.3 pH units from pH 6.8 $\pm$ 0.2 to pH 6.1 $\pm$ 0.3 and from pH 6.7 $\pm$ 0.4 to pH 6.4 $\pm$ 0.4 in the 4T1 and HeLa tumor samples, respectively.

Discussion

Hypoxic conditions induce a switch from the oxidative–phosphorylation mechanism of energy production to glycolysis. In addition,

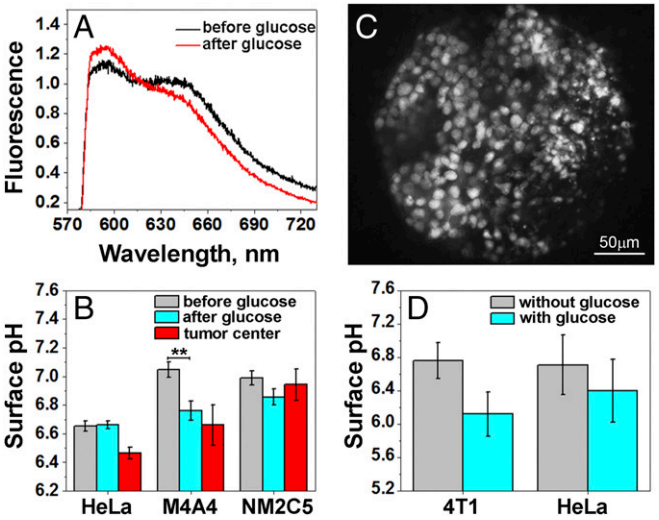

Fig. 3. pH measured at the surfaces of cancer cells in tumors in vivo and ex vivo. (*A*) Representative fluorescence spectra recorded from tumors in live mice (skin is removed from the tumor site) 4 h after administration of SNARF-pHLIP as a single tail vein injection before and after i.p. injection of 125 mg of glucose. (*B*) Mean values of cell surface pH at the surface of a tumor of a live animal before and after injection of glucose (in vivo measurements) and in the middle of the excised tumor after glucose injection (ex vivo measurements). The number of measurements that were performed on multiple HeLa tumors before and after glucose injection and in the tumor center were 24, 30, and 36, respectively; on M4A4 tumors before and after glucose injection and in the tumor center were 13, 11, and 10, respectively; and on NM2C5 tumors before and after glucose injection and in the tumor center were 16, 21, and 8, respectively. $^{**}P < 0.005$. (*C*) Representative fluorescence image obtained from a HeLa tumor specimen treated ex vivo with the SNARF-pHLIP in the presence of glucose, followed by washing. (*D*) Mean values of the surface pH measured ex vivo in HeLa and 4T1 tumor specimens treated with the SNARF-pHLIP in the absence and presence of glucose. The measurements performed on the HeLa tumor specimens in the absence and presence of glucose were 56 and 51, respectively; and on the 4T1 tumor specimens in absence and presence of glucose were 35 and 31, respectively.

malignant cancers have an elevated glucose uptake even under normal oxygen conditions, known as the Warburg effect (4–6). Each of these mechanisms results in an elevated level of H^+ and lactic acid production in the cytoplasm. To maintain cytoplasmic pH, these byproducts are pumped across the plasma membrane into the extracellular space, where they accumulate in poorly perfused regions such as solid tumors and ischemic stroke lesions (45–48). In tumors, the rapid metabolism produces high levels of CO_2, inducing the expression of cell surface carbonic anhydrases, which catalyze the production of additional extracellular acid by hydrating cell-generated CO_2 into HCO_3^- and H^+ (7, 8). These mechanisms each contribute to an acidic extracellular milieu and create an "acidic crown" around cancer cells that favors tumor development and progression, playing a role in almost all steps of metastasis: more acidic tumors became highly aggressive and metastatic (11). The pH near tumor cell surfaces is the lowest, and acidity decays with distance (19). Thus, the pH at cell surfaces can be a measure of the stage of tumor development.

Acidification of extracellular space associated not only with tumor development but also with other pathological states, such as ischemic stroke, neurotrauma, epileptic seizure, inflammation, infection, wounds, and others (1–3). Previously, we have demonstrated targeting of inflammatory arthritis (28) and ischemic myocardium (34) by fluorescent pHLIPs.

The SNARF-pHLIP tool enables pH measurement at the surfaces of cells in acidic diseased tissues. We have validated the method on metastatic and nonmetastatic cancer cells grown in tumor spheroids and in mouse tumor models. The mean values of pH at the surfaces of cancer cells in the center of highly metastatic (HeLa and M4A4) tumors were found to be 6.5–6.7, whereas the average pH at the surfaces of cancer cells in nonmetastatic tumors (NM2C5) was 6.9. The values obtained are about 0.2–0.4 pH units lower than the pH values of the bulk extracellular space measured by ^{31}P MRS in various mouse and rat tumor models, variously reported as pH 6.7 to pH 7.0 (the normal tissue pH was established to be 7.3–7.4) (49). The new measurement is sensitive enough to detect 0.2 pH unit decreases induced by glucose injection. The distribution of surface pH within a tumor mass was heterogeneous, with the lowest values found to be 6.0–6.1. We speculate that these parts may contain the most aggressive and invasive subpopulation of cancer cells.

Using our new probe, we have shown that the pH at the surfaces of cancer cells, especially metastatic cells, can be 0.7–0.9 pH units lower than the pH, typically 7.4, of the bulk fluids in normal tissues. This finding indicates that cancer cells can be detected not only in poorly perfused parts of a diseased tissue but also in well-perfused tissue and biofluids. An ability to measure surface pH might have clinical applications for diagnostic surface pH measurements of cancer cells in human biopsy specimens, blood, and other biofluids. Because surface acidity correlates with tumor stage and invasiveness, pH measurements may usefully guide therapeutic choices, serve as therapeutic monitors, or aid therapeutic agent research and development.

Materials and Methods

Peptide Synthesis and Conjugation with Fluorescent Dyes. A pHLIP was synthesized with a single Lys residue near its acetylated N-terminus (Ac-AKEQNPIYWARYADWLFTTPLLLLDLALLVDADEGT) and purified by reverse-phase chromatography by CS Bio. SNARF-1 carboxylic acid, acetate, succinimidyl ester (Life Technologies) were incubated at a ratio of 2:1 with the pHLIP in 60% (vol/vol) dimethylformamide, 30% (vol/vol) 0.1 M PBS pH 9.0, and 10% (vol/vol) pH 9.5 0.1 M sodium bicarbonate buffer for a final pH of 9.0. SNARF-1 was converted to its fluorescent form after conjugation by raising the conjugation solution's volume by 50% (vol/vol) with methanol and raising the solution pH to 12 with 2 M potassium hydroxide for 1 h, then pH was adjusted to 7.0 by adding 1M HCl. The reaction progress was monitored by reverse-phase (Zorbax SB-C18 columns; 9.4 × 250 mm; 5 μm; Agilent Technology) HPLC using a gradient of 25–75% acetonitrile and water containing 0.05% trifluoroacetic acid. The concentration of each labeled peptide in buffer was determined by SNARF-1 absorption at 548 nm, ε_{548} = 27,000 M^{-1} cm^{-1}. The purity and characterization of the constructs was performed by analytical HPLC and surface-enhanced laser desorption/ionization–TOF mass spectrometry.

Phosphate-Buffered Solutions. Phosphate-buffered solutions were prepared by mixing 0.5 M dibasic and monobasic solutions (J. T. Baker) to obtain the desired pH in the range of 5.5–8.0. The final PBS solutions (experimental PBS) contained 10 mM phosphate, 150 mM NaCl (J. T. Baker), 0.2 mM $MgCl_2$ (Sigma), and 0.2 mM $CaCl_2$ (Sigma). The pH of the final solution was measured with a microelectrode pH meter (Thermo Scientific). Buffer solutions were sterilized by passage through a 0.2-μm filter.

Liposome Preparation. Large unilamellar vesicles (LUVs) were prepared by extrusion; 2.5 mg of POPC (Avanti Polar Lipids) lipids were dissolved in 0.5 mL of chloroform, desolvated on a rotary evaporator, and dried under high vacuum for 3 h. The phospholipid film was then rehydrated in pH 7.4 experimental PBS, vortexed for 5 min, and repeatedly extruded through a membrane with 50-nm pores to obtain LUVs.

Cell Lines. Human cervical adenocarcinoma HeLa, human melanoma M4A4, human melanoma NM2C5, and mouse breast cancer 4T1 cell lines were purchased from the American Tissue and Culture Collection (ATCC). All lines were propagated in Dulbecco's modified Eagle medium (DMEM) containing 4.5 g/L D-glucose and 40 mg/L sodium pyruvate supplemented with 10% FBS (Gibco), ciprofloxacin·HCl (10 μg/mL) (from Cellgro, Voigt Global Distribution) in a humidified atmosphere of 5% CO_2 at 37 °C.

Tumor Spheroids. A total of 150 μL of 1% agarose (Sigma) in 1× strength PBS pH 7.4 (Gibco) was pipetted into each well of a 48-well flat bottom tissue culture plate (Celltreat). After the agarose gel had sufficiently settled (~1 h), 200 μL of DMEM supplemented with 10% FBS, ciprofloxacin·HCl was then added to each well. The covered tray was then left in a humidified atmosphere at 37 °C, 5% CO_2 for 24 h. Next, a suctioned glass Pasteur pipette was used to remove excess media from the agarose layer. Then, 200 μL of the same DMEM with 10,000 HeLa, NM2C5, or M4A4 cells were seeded into each well and kept in a humidified atmosphere of 5% CO_2 at 37 °C for 3–4 d. When matrigel (Corning) was used, it was dissolved on ice in DMEM at a concentration of 2.5% (to give 2% once added to the wells) and then heated to 37 °C before being combined with cells to be seeded.

Tumor Mouse Models. All animal studies were conducted according to the animal protocol AN04-12-011 approved by the Institutional Animal Care and Use Committee at the University of Rhode Island, in compliance with the principles and procedures outlined by the NIH for the Care and Use of Animals. s.c. tumors were established by injection of HeLa (1.5×10^6 cells per 0.1 mL per flank), M4A4 (1.5×10^6 cells per 0.1 mL per flank), NM2C5 (2×10^6 cells per 0.1 mL per flank), and 4T1 cells (0.8×10^6 cells per 0.1 mL per flank) in the right flank of adult female athymic nude mice (for implanting of human cancer cell lines: HeLa, M4A4, and NM2C5) and adult female BALB/c mice (for implanting of murine cancer cell line 4T1). Mice were about 20–22 g and were obtained from Harlan Laboratories.

Imaging Tumor Spheroids. The spheroids of a given cell line were incubated with 5 μM SNARF-pHLIP in 50 μL of experimental PBS buffer (pH 6.3) either with 25 mM D-glucose (glucose) or 50 mM 2DG, in an open Eppendorf in a humidified atmosphere of 5% CO_2 at 37 °C for 30 min. The spheroids were then washed three times with 1 mL of experimental PBS of the pH that was desired for the observation. The spheroids were then placed into an open Eppendorf with 1 mL of the same PBS, followed by washing with PBS containing either 25 mM glucose or 50 mM 2DG for 15 min. The spheroids were transferred to a single well of a glass-bottom 96-well cell tray, and the fluorescence signal was recorded through an inverted epifluorescence microscope (Olympus IX71) (mostly using a 20× objective lens). Both spectra and images of the SNARF-pHLIP from tumor spheroids were obtained using the same excitation filter (FF01-531/40-25; Semrock) with a band of transmittance at 531 ± 20 nm. The fluorescence spectra from tumor spheroids were recorded by Solis software (Andor) after emission from the sample was passed through a long-pass emission filter (BCP01-568R-25; Semrock) with transmittance at 580 nm and higher and a Shamrock SR-303i-B spectrograph (Andor) with a diffraction grating of 300 lines per millimeter with 500-nm blaze wavelength, a 400-μm entrance slit, and a Newton^{EM} electron-multiplying CCD camera (Andor) thermoelectrically cooled to −60 °C. Spectra were taken every several minutes until three in a row were identical at the noise level. After recording the spectra, fluorescent images of the samples were acquired using Qcapture software by a Retiga-SRV CCD (Qimaging)

with two emission filters FF01-580/14-25 (Semrock) and FF01-640/14-25 (Semrock) with transmittance at 580 ± 7 nm and 640 ± 10 nm, respectively.

SNARF-pHLIP Liposome Calibration. A total of 300 μL of 1 μM SNARF-pHLIP and 200 μM POPC liposomes were mixed into pH 7.4 experimental PBS and left to incubate overnight at 4 °C. The pH was adjusted by adding 0.5 M hydrochloric acid or 2 M potassium hydroxide, and final pH of the solution was measured with a microelectrode pH meter (Thermo Scientific). The solution was placed into a glass-bottom collagen-coated cell dish (MatTek) and imaged on a fluorescence microscope with an 20× objective lens. Spectra were taken as described above.

Trypan Blue Assay. Trypan blue solution (Sigma) at a concentration of 0.67 M in experimental PBS (pH 7.0) was added to a HeLa spheroid, which was incubated with SNARF-pHLIP as described above, in a glass-bottom collagen-coated cell dish (MatTek). The fluorescence spectra and images before and immediately after addition of Trypan blue were taken as described above using a 20× objective lens.

In Vivo Imaging of Tumors. When tumors reached 5–8 mm in diameter, each mouse was restricted from eating for 24 h before a single tail vein injection of 4 nmol (100 μL of 40 μM) of SNARF-pHLIP in PBS was performed. At 4 h after injection, the skin was removed from the tumor site under ketamine/xylazine anesthesia, and the mouse tumor was placed onto a 24 × 60-mm No.1 thickness glass slide and imaged using a fluorescence microscope using a 20× magnification objective lens, as described above. The SNARF-pHLIP fluorescence spectra and images were taken from various areas of the tumor before and after an i.p. injection of 125 mg of glucose (125 mg in 220 μL of PBS pH 7.4). After in vivo imaging, each animal was euthanized by cervical dislocation, and the tumor was excised and cut in half, and fluorescence spectra and images were acquired immediately as described above.

Ex Vivo Imaging of Tumors. When its tumor reached 5–8 mm in diameter, each mouse was euthanized and the tumor was excised. The tumor was cut into slices and placed into 150 μL of 1 μM solution of SNARF-pHLIP in PBS (pH 6.3) with either no glucose or 25 mM glucose. The slices were left to incubate with SNARF-pHLIP for 1 h and washed three times with 150 μL of experimental PBS (pH 7.4) with 15 min between washings. The slices were placed into a glass-bottom dish, and spectra and images were acquired.

Spectra and Image Analysis. The fluorescence spectra were analyzed with a Mathematica program (Version 10; Wolfram). All graphs were constructed using Origin Lab (Version 9.1; Origin Lab Corporation). *P* values were computed based on the two-tailed test.

ACKNOWLEDGMENTS. We thank Dr. Ramona-Cosmina Adochite, Dr. Gregory Andreev, Mr. Linden Wyatt, and Mr. Da Wei for assistance with the pH-imaging project. This work was supported by NIH Grants CA174413 (to O.A.A. and Y.K.R.) and GM073857 (to O.A.A., Y.K.R., and D.M.E.).

1. Pezzulo AA, et al. (2012) Reduced airway surface pH impairs bacterial killing in the porcine cystic fibrosis lung. *Nature* 487(7405):109–113.
2. Paschen W, Djuricic B, Mies G, Schmidt-Kastner R, Linn F (1987) Lactate and pH in the brain: Association and dissociation in different pathophysiological states. *J Neurochem* 48(1):154–159.
3. Kedika RR, Souza RF, Spechler SJ (2009) Potential anti-inflammatory effects of proton pump inhibitors: A review and discussion of the clinical implications. *Dig Dis Sci* 54(11):2312–2317.
4. Warburg O, Wind F, Negelein E (1927) The metabolism of tumors in the body. *J Gen Physiol* 8(6):519–530.
5. Gillies RJ, Robey I, Gatenby RA (2008) Causes and consequences of increased glucose metabolism of cancers. *J Nucl Med* 49(Suppl 2):24S–42S.
6. Newell K, Franchi A, Pouysségur J, Tannock I (1993) Studies with glycolysis-deficient cells suggest that production of lactic acid is not the only cause of tumor acidity. *Proc Natl Acad Sci USA* 90(3):1127–1131.
7. Swietach P, Vaughan-Jones RD, Harris AL (2007) Regulation of tumor pH and the role of carbonic anhydrase 9. *Cancer Metastasis Rev* 26(2):299–310.
8. Ihnatko R, et al. (2006) Extracellular acidosis elevates carbonic anhydrase IX in human glioblastoma cells via transcriptional modulation that does not depend on hypoxia. *Int J Oncol* 29(4):1025–1033.
9. Gerweck LE, Seetharaman K (1996) Cellular pH gradient in tumor versus normal tissue: Potential exploitation for the treatment of cancer. *Cancer Res* 56(6):1194–1198.
10. Raghunand N, et al. (1999) Plasmalemmal pH-gradients in drug-sensitive and drug-resistant MCF-7 human breast carcinoma xenografts measured by 31P magnetic resonance spectroscopy. *Biochem Pharmacol* 57(3):309–312.
11. Hashim AI, Zhang X, Wojtkowiak JW, Martinez GV, Gillies RJ (2011) Imaging pH and metastasis. *NMR Biomed* 24(6):582–591.
12. Chiche J, Brahimi-Horn MC, Pouysségur J (2010) Tumour hypoxia induces a metabolic shift causing acidosis: A common feature in cancer. *J Cell Mol Med* 14(4):771–794.
13. Parks SK, Chiche J, Pouysségur J (2013) Disrupting proton dynamics and energy metabolism for cancer therapy. *Nat Rev Cancer* 13(9):611–623.
14. Zhang S, Wu K, Sherry AD (1999) A novel pH-sensitive MRI contrast agent. *Angew Chem Int Ed Engl* 38(21):3192–3194.
15. Zhang X, Lin Y, Gillies RJ (2010) Tumor pH and its measurement. *J Nucl Med* 51(8):1167–1170.
16. Gallagher FA, et al. (2008) Magnetic resonance imaging of pH in vivo using hyperpolarized 13C-labelled bicarbonate. *Nature* 453(7197):940–943.
17. Gallagher FA, Kettunen MI, Brindle KM (2011) Imaging pH with hyperpolarized 13C. *NMR Biomed* 24(8):1006–1015.
18. Helmlinger G, Yuan F, Dellian M, Jain RK (1997) Interstitial pH and pO2 gradients in solid tumors in vivo: High-resolution measurements reveal a lack of correlation. *Nat Med* 3(2): 177–182.
19. Stock C, et al. (2007) pH nanoenvironment at the surface of single melanoma cells. *Cell Physiol Biochem* 20(5):679–686.
20. Schreml S, et al. (2011) 2D luminescence imaging of pH in vivo. *Proc Natl Acad Sci USA* 108(6):2432–2437.
21. Hilderbrand SA, Kelly KA, Niedre M, Weissleder R (2008) Near infrared fluorescence-based bacteriophage particles for ratiometric pH imaging. *Bioconjug Chem* 19(8):1635–1639.
22. Gatenby RA, Gawlinski ET, Gmitro AF, Kaylor B, Gillies RJ (2006) Acid-mediated tumor invasion: A multidisciplinary study. *Cancer Res* 66(10):5216–5223.
23. Ke G, et al. (2014) A cell-surface-anchored ratiometric fluorescent probe for extracellular pH sensing. *ACS Appl Mater Interfaces* 6(17):15329–15334.
24. Weerakkody D, et al. (2013) Family of pH (low) insertion peptides for tumor targeting. *Proc Natl Acad Sci USA* 110(15):5834–5839.
25. Andreev OA, Engelman DM, Reshetnyak YK (2014) Targeting diseased tissues by pHLIP insertion at low cell surface pH. *Front Physiol* 5:97.
26. Reshetnyak YK, Andreev OA, Lehnert U, Engelman DM (2006) Translocation of molecules into cells by pH-dependent insertion of a transmembrane helix. *Proc Natl Acad Sci USA* 103(17):6460–6465.
27. Reshetnyak YK, Segala M, Andreev OA, Engelman DM (2007) A monomeric membrane peptide that lives in three worlds: In solution, attached to, and inserted across lipid bilayers. *Biophys J* 93(7):2363–2372.
28. Andreev OA, et al. (2007) Mechanism and uses of a membrane peptide that targets tumors and other acidic tissues in vivo. *Proc Natl Acad Sci USA* 104(19):7893–7898.
29. Karabadzhak AG, et al. (2012) Modulation of the pHLIP transmembrane helix insertion pathway. *Biophys J* 102(8):1846–1855.
30. Vävere AL, et al. (2009) A novel technology for the imaging of acidic prostate tumors by positron emission tomography. *Cancer Res* 69(10):4510–4516.
31. Reshetnyak YK, et al. (2011) Measuring tumor aggressiveness and targeting metastatic lesions with fluorescent pHLIP. *Mol Imaging Biol* 13(6):1146–1156.
32. Daumar P, et al. (2012) Efficient (18)F-labeling of large 37-amino-acid pHLIP peptide analogues and their biological evaluation. *Bioconjug Chem* 23(8):1557–1566.
33. Macholl S, et al. (2012) In vivo pH imaging with (99m)Tc-pHLIP. *Mol Imaging Biol* 14(6): 725–734.
34. Sosunov EA, et al. (2013) pH (low) insertion peptide (pHLIP) targets ischemic myocardium. *Proc Natl Acad Sci USA* 110(1):82–86.
35. Adochite RC, et al. (2014) Targeting breast tumors with pH (low) insertion peptides. *Mol Pharm* 11(8):2896–2905.
36. Cruz-Monserrate Z, et al. (2014) Targeting pancreatic ductal adenocarcinoma acidic microenvironment. *Sci Rep* 4:4410.
37. Karabadzhak AG, et al. (2014) pHLIP-FIRE, a cell insertion-triggered fluorescent probe for imaging tumors demonstrates targeted cargo delivery in vivo. *ACS Chem Biol* 9(11):2545–2553.
38. Suzuki M, Mose ES, Montel V, Tarin D (2006) Dormant cancer cells retrieved from metastasis-free organs regain tumorigenic and metastatic potency. *Am J Pathol* 169(2):673–681.
39. Rae JM, et al. (2004) Common origins of MDA-MB-435 cells from various sources with those shown to have melanoma properties. *Clin Exp Metastasis* 21(6):543–552.
40. Loike JD, Silverstein SC (1983) A fluorescence quenching technique using trypan blue to differentiate between attached and ingested glutaraldehyde-fixed red blood cells in phagocytosing murine macrophages. *J Immunol Methods* 57(1-3):373–379.
41. Elamrani K, Blume A (1983) Effect of the lipid phase transition on the kinetics of H+/OH- diffusion across phosphatidic acid bilayers. *Biochim Biophys Acta* 727(1):22–30.
42. Ibrahim-Hashim A, et al. (2011) Free base lysine increases survival and reduces metastasis in prostate cancer model. *J Cancer Sci Ther* 4(Suppl 1):JCST-S1-004.
43. Kozin SV, Shkarin P, Gerweck LE (2001) The cell transmembrane pH gradient in tumors enhances cytotoxicity of specific weak acid chemotherapeutics. *Cancer Res* 61(12):4740–4743.
44. Jähde E, Rajewsky MF (1982) Tumor-selective modification of cellular microenvironment in vivo: Effect of glucose infusion on the pH in normal and malignant rat tissues. *Cancer Res* 42(4):1505–1512.
45. Grillon E, et al. (2011) The spatial organization of proton and lactate transport in a rat brain tumor. *PLoS One* 6(2):e17416.
46. Rehncrona S (1985) Brain acidosis. *Ann Emerg Med* 14(8):770–776.
47. Xiong ZG, Pignataro G, Li M, Chang SY, Simon RP (2008) Acid-sensing ion channels (ASICs) as pharmacological targets for neurodegenerative diseases. *Curr Opin Pharmacol* 8(1):25–32.
48. Shulman RG, Rothman DL (2015) Homeostasis and the glycogen shunt explains aerobic ethanol production in yeast. *Proc Natl Acad Sci USA* 112(35):10902–10907.
49. Gillies RJ, Raghunand N, Karczmar GS, Bhujwalla ZM (2002) MRI of the tumor microenvironment. *J Magn Reson Imaging* 16(4):430–450.